Soft Matter

RSC Publishing

PAPER

View Article Online
View Journal | View Issue

Cite this: *Soft Matter*, 2013, **9**, 6955

Complexation between weakly basic dendrimers and linear polyelectrolytes: effects of grafts, chain stiffness, and pOH

Thomas Lewis, Gunja Pandav, Ahmad Omar and Venkat Ganesan*

Received 7th January 2013
Accepted 27th March 2013

DOI: 10.1039/c3sm00062a

www.rsc.org/softmatter

We develop and implement a new hybrid methodology combining self-consistent field theory (SCFT) and Monte Carlo simulations to study the complexation between negatively charged semiflexible linear polyelectrolyte (LPE) molecules and a positively charged dendrimer containing grafts of neutral polymers. We examine the influence of LPE stiffness, length of the dendrimer grafts, and solution pOH upon the characteristics of the resulting complexes. Our results indicate that increasing LPE stiffness reduces the dendrimer–LPE binding affinity and results in an overall higher net charge carried within the dendrimer molecule. When we varied the size of the grafts, the dendrimer–LPE binding strength was seen to decrease with increasing grafting chain length for the flexible LPE chains. In contrast, for stiff LPE chains, the binding strength was not seen to vary significantly with the grafting lengths. Overall, longer grafting lengths were seen to reduce the fraction of exposed LPE molecules, suggesting that grafted dendrimers may better shield nucleic acid material from serum nucleases. Lastly, we found that increasing the solution pOH was seen to enhance both the binding between the dendrimer and LPE molecules and the total positive charge carried by the complex.

1 Introduction

Gene therapy involves the application of therapeutic nucleic acid (NA) materials to manipulate gene expression of targeted cells. Advances in biomedical research have yielded effective gene therapy agents that not only include large plasmids, but also shorter single and double stranded oligomers (*e.g.* antisense oligonucleotides, siRNA, and DNAzymes) of varying flexibility.[1–13] Successful gene therapy requires the transport of genetic material to targeted cells, permeation of the cell membrane, and endosomal escape before the onset of lysosomal degradation. Serum nucleases in the blood stream rapidly degrade unshielded genetic material, and the negative charge of the NAs hinders their ability to permeate the negatively charged cell membrane. To overcome these challenges, researchers have proposed the use of cationic polymer molecules as gene delivery vectors for NA material. Dendrimers, regularly branched tree-like polymer molecules, which carry amine groups have shown great promise as efficient gene vectors,[1–13] and advances in their synthesis techniques have allowed researchers to produce highly monodisperse molecules, with precise control over their size, solubility, flexibility, charge, and functionality.[14–16] Concomitantly, a number of experiments have demonstrated that by controlling one or more of such synthesis parameters, the transfection ability of dendrimers can potentially be optimized against their cytotoxicity.[1,3–9,11–13] As a result, there is presently an active interest in developing a fundamental understanding on the influence of design characteristics of dendrimer molecules upon their transfection efficiencies.

As a consequence of the vast parameter space available for synthetic chemists, theoretical models and computer simulations have emerged as an attractive means to study complexation phenomena involving dendrimers and model NA materials.[17] The most detailed studies in this regard have used atomistic molecular dynamics (MD) simulations to study the phenomenology of dendrimer–DNA binding.[18–23] While such studies have provided valuable insights the binding between dendrimers and NA materials, identification of the physical principles underlying complexation phenomena over a broad parameter space is very computationally expensive in such methodologies. Motivated by these limitations, a number of coarse-grained simulations have modeled the NA material as either a flexible or a semiflexible linear polyelectrolyte (LPE) and studied the physics of their binding with dendrimers.[24–31] For instance, Welch and Muthukumar used a Monte Carlo (MC) methodology to study the complexes formed between dendrimers and LPEs.[24] They observed different possibilities for complexation such as the complete encapsulation of the LPE, partial interpenetration between LPE and the dendrimer, *etc.* Lyulin and coworkers performed a series of Brownian dynamics

Department of Chemical Engineering, University of Texas at Austin, Austin, TX 78712, USA. E-mail: venkat@che.utexas.edu

simulation studies on the influence of the dendrimer/NA charge ratio upon the overall charge of the dendrimer–LPE complexes.[25–28] They observed that when the charge carried by the LPE molecule exceeded that of the dendrimer molecule, an excess of charged LPE molecules were adsorbed by the dendrimer (overcharging).

More recent studies have examined the effect of LPE rigidities upon the relevant physics of binding. For example, Tian and Ma[29] used coarse-grained MD simulations and observed a decrease in dendrimer–LPE contacts as LPE stiffness increased. Klos and Sommer applied MC simulations to examine the effects of LPE rigidity and chain length on the complexation with non-grafted charged dendrimers under a wide variety of bending energies and electrostatic parameters.[31] Their work demonstrated that dendrimer–LPE complexes (dendriplexes) could be stable even for very stiff chains if the electrostatic interactions are strong enough.

Despite the vast number of theoretical and simulation studies which have studied the binding between dendrimers and linear polyelectrolytes, a few outstanding issues remain which motivated the work we report in this article:

1.1 Influence of polymer grafts on the dendrimer–LPE complexation

A number of experimental studies have shown that the transfection efficiency of dendrimers is enhanced with increasing dendrimer generation, an effect which has been attributed to the increase in charge carried by the larger generation dendrimers.[1,2,8] However, an enhancement of the positive charges carried by the dendrimers also leads to the formation of holes in the anionic cellular membrane, an effect which is cytotoxic.[32–34] To combat this phenomena, researchers have pursued modification of the dendrimers by covalent conjugation of poly(ethylene glycol) (PEG) chains to the periphery of the dendrimer molecules.[9–13] For instance, Tack *et al.* examined the effect of PEGylation of the peripheral amines upon the transfection of PPI dendrimer–DNAzyme complexes, and observed that PEGylated dendrimers exhibited high transfection efficiencies.[11] Later studies by Fant *et al.* demonstrated that PEGylation of poly(amidoamine) (PAMAM) dendrimers decreased the binding affinity between the PEGylated dendrimers and the plasmid DNA.[9,10] The latter has been suggested to be beneficial for the dissociation of the dendrimer complex once inside of the cellular cytoplasm, a necessary step for successful gene transfection.[3,9,10] While a number of works have elucidated the effect of neutral grafts on the structure and dynamics of both charged and uncharged dendrimer molecules,[35–37] there is still a lack of understanding on how dendrimer grafts influence the complexation of dendrimers with LPEs. Some outstanding questions in this regard are: how does the grafting length affect the LPE–dendrimer binding strength? How do grafts affect the shielding/exposure of the LPE molecules? What is the role of grafts upon the resulting dendriplex charges?

1.2 The role of solution pH on dendrimer–LPE complexation

In the course of transfection, dendriplexes are exposed to a variety of pH environments. For instance, dendriplexes within the endosome face a low pH environment, leading to the adsorption of H^+ ions by the dendrimer and creating an osmotic pressure, which results in the rupture of the membrane.[6,38] While previous LPE–dendrimer simulations have studied the influence of pH changes upon the properties of dendriplexes by modulating the number of charged monomers,[18,20,23,27] an accurate model for weak polyelectrolytes needs to account for acid–base equilibrium effects and their simultaneous influence on LPE binding and conformations. For instance, in a recent work we compared the conformations of weak and strong polyelectrolyte dendrimers and noted several differences arising from the capability of the former to tune the dissociation of charges in response to their conformation and interactions.[39] To our knowledge, there have not been any studies which have examined the influence of such acid–base equilibrium considerations in the context of pH changes to delineate their influence upon the binding between dendrimers and linear polyelectrolytes.

Motivated by the above shortcomings, we report results from coarse-grained modeling of grafted weakly basic dendrimer molecules and charged LPE molecules. In order to elucidate the effect of design parameters on dendriplex formation, we develop a new hybrid approach which combines self-consistent field theory (SCFT) and Monte Carlo simulation. In contrast to an explicit MC or MD simulation of the dendrimer, the LPE, and counterion species, the methodology we propose provides an expedited approach to access the equilibrium thermodynamics of the system as well as the conformational features of the LPEs. Using such a framework, we examine the effects of dendrimer grafting length, polyelectrolyte chain stiffness, and solution pOH on the dendriplex and LPE chain conformations. The rest of the article is arranged as follows. In Section 2 we discuss our hybrid SCFT–MC model and the associated terminology. In Section 3, we present results that examine the effect of LPE stiffness (Section 3.1), grafting length (Section 3.2), and solution pOH (Section 3.3). In Section 4 we conclude with a summary of our results.

2 Hybrid self-consistent field theory and Monte Carlo approach

As mentioned in the introduction, we develop and apply a hybrid SCFT-MC methodology to study the characteristics of dendrimer–LPE complexes. In a nutshell, the framework of polymer SCFT enumerates the statistical features of an interacting system of polymer chains by considering an equivalent system of noninteracting chains in the presence of pseudo chemical potential fields.[40] These chemical potential fields are further determined in a self-consistent manner to impose the inhomogeneous densities of the appropriate components. Using such a methodology, a density functional theory for the system free energy can be constructed which allows one to deduce the equilibrium composition profiles (*i.e.* morphologies).

Polymer SCFT allows us to determine the equilibrium density profiles of the dendrimer, LPE, counterions and salt components for specified conditions of dendrimer architecture, LPE stiffness, and solution pOH. However, SCFT by itself is incapable of providing information on certain quantities of

interest (*e.g.* conformational features such as the radius of gyration and the center of mass distributions of the LPE chains). As a means to access such features, we use the SCFT chemical potential fields as input to MC simulations of non-interacting LPE chains. From the MC simulations, we determine the conformational properties of the LPE chains, specifically, the LPE center of mass (COM) densities and the loop/tail distributions of the complexed LPEs. In our MC simulations, we significantly reduce the system degrees of freedom and the associated computational costs by only considering interactions between individual chains and the SCFT fields. This approach allows us to obtain as much information about the LPEs as would be available by using a much more computationally intensive MC or MD simulation involving all the species in the system. Below we present a more detailed description of the SCFT model and the MC simulation approach.

2.1 Self-consistent field theory model

Our model system is composed of a dendrimer (P) and its grafts (G) in the presence of linear polyelectrolyte molecules (LPE), solvent molecules (S), H^+ and OH^- ions, and monovalent salt ions (denoted as Na^+ and Cl^-). Fig. 1a presents a schematic representation of a "third generation" dendrimer (black) with neutral grafted chains (red) attached at the periphery. The 0^{th} generation is comprised of the core monomer and the three stemming branches, and the next generation of dendrimers is comprised of the spacers attached at the end groups of the 0^{th} generation. The "functionality" of the branches denote the number of branches stemming from an individual branch point, and in this notation, the number of monomers, M, comprising a non-conjugated dendrimer molecule is given by:

$$M(g) = nf((f-1)^{g+1} - 1) + 1 \quad (1)$$

where n is the number of monomers per spacer, f is the branch point functionality, and g is the generation number. We assume that every terminal group of the dendrimer molecule is grafted with a polymer of length N_G such that the number of monomers in the graft portion of the dendrimer molecule is given as:

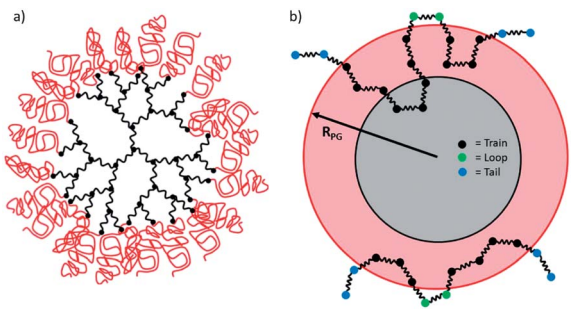

Fig. 1 (a) Schematic of a grafted 3^{rd} generation dendrimer having a functionality of 3. The dendrimer portion is represented in black, while the grafted portions are represented in red. (b) Schematic visualizing the definition of trains, loops, and tails as measured at the R_{PG} boundary.

$$M_G(g) = N_G f(f-1)^g. \quad (2)$$

We note that during PEGylated dendrimer synthesis, complete PEGylation of the dendrimer primary amines is unlikely to occur due to the steric interactions resulting from PEGylation.[3,41] However, to simplify our SCFT framework and the number of parameters involved, we assume that every end group of the dendrimer is PEGylated.

Our system is spherically symmetric, with the core dendrimer monomer constrained to the center. In modeling our system, we make the following assumptions:

(i) We model the dendrimer spacers and neutral grafts as flexible continuous Gaussian chains. We note that in reality, the flexibility of dendrimer spacers is dependent upon the chemistry of the dendrimer monomers.[14] Although previous studies have found that the flexibility of dendrimer molecules affects their conformations[42–44] and binding affinities with genetic material,[45] we treat the spacers as flexible chains in this study to simplify our model and parameter sweep.

(ii) The flexibility of the LPE molecules has been shown to affect dendrimer–LPE complexation.[29,31] In this study, we assume that the chain is semiflexible and use the wormlike chain model to describe their conformations.[40] To account for the conformations of the LPE molecules in a spherically symmetric cell, we use a recently developed SCFT framework to access the information of semiflexible polymers in a spherically symmetric system (also see Appendix).[46]

(iii) We assume that electrostatic interactions are the main attractive forces driving the complexation between the dendrimer and LPE molecules. Thus, we do not include any other enthalpic terms that account for hydrophobic interaction or hydrogen bonding between the dendrimers and LPE. The electrostatic interactions between charged molecules and ions in our system are modeled using a classical Coulomb potential[40] with a spatially constant dielectric value.

(iv) We model the total density of the overall system as almost uniform by including a harmonic compressibility penalty for deviations of the local density from the average density, ρ_0.[47–49]

(v) We model the charge dissociation of the dendrimer monomers using an approach similar to that adopted by Szleifer *et al.*[50–52] and Won and co-workers.[53,54] Explicitly, we assume that a fraction, α_P, of the dendrimer monomers carry dissociable charge groups and are capable of becoming charged through the equilibrium reaction:

$$P + H_2O \rightleftharpoons PH^+ + OH^-. \quad (3)$$

In a dilute solution of the dendrimer monomers, the equilibrium fraction of charged monomers, α_b, can be determined through the law of mass action:

$$K_{b,P} = \frac{[PH^+][OH^-]}{[P]} = \frac{\alpha_b \rho_0 \varphi_{OH^-,b}}{1-\alpha_b}, \quad (4)$$

where $K_{b,P}$ denotes the equilibrium constant of the dissociation reaction (eqn (3)), [X] (X ≡ P, PH^+, OH^-) refers to the

concentration in mol L^{-1} of species X, ρ_0 is the density of a single monomer, and $\varphi_{OH^-,b}$ is the bulk volume fraction of OH^- ions. The equilibrium constant $K_{b,P}$ is proportional to $\exp(-\beta\Delta G^o)$, where $\Delta G^o = \gamma^o_{OH^-} + \gamma^o_{PH^+} - \gamma^o_P$ is the free energy of the reaction, and γ^o_i are the standard chemical potentials of the different species involved in the dissociation reaction. To reduce parametric complexity, we assume that α_P does not change when comparing grafted and non-grafted dendrimers. However, in reality the addition a PEG chain to a dendrimer converts a primary surface amine to an amide bond, which strongly reduces its ability to absorb a hydrogen ion. Thus, our results that compare grafted and non-grafted dendrimers are equivalent to comparing PEGylated and acetylated dendrimers that have the same number of reacted terminal monomers.

(vi) We model the charge on the LPE by using a fixed charge model, where every monomer along the chain carries a charge of $z_{LPE} = -1.0$. This is expected to be reasonable since the phosphate groups present in phosphate-ribose/deoxyribose backbones of RNA and DNA have pK_a values near 0. Thus they are strong acids and will be almost completely charged at physiological conditions.

Using the above assumptions, we develop an equilibrium thermodynamic model for the free energy of the system containing the dendrimer, grafts, solvent, ions, and LPE molecules (see the Appendix for more details). We model the free energy as a functional of the local volume fractions, $\varphi_i(r)$, and the conjugate chemical potentials, $w_i(r)$, where i denotes the P, G, S, H^+, OH^-, Na^+, Cl^-, and LPE species. We then minimize the free energy with respect to the volume fraction and chemical potential fields to obtain a set of self-consistent equations, the solution of which yields the equilibrium density profiles within a mean field approximation. In addition to determining $\varphi_i(r)$, we also characterize the conformations of the LPE chains through an orientational order parameter, $S(r)$ defined as

$$S(r) = \left\langle \frac{3\cos^2\theta(r) - 1}{2} \right\rangle, \tag{5}$$

where $\theta(r)$ denotes the angles formed between the radial vector emanating from the dendrimer center and the LPE bond vectors, and $\langle\cdots\rangle$ denotes an average over the LPE conformations. Complete ordering of the LPE bonds in a tangential orientation (along the θ axis) corresponds to the case where $S(r) = -0.5$, whereas complete alignment with the radial axis corresponds to the case where $S(r) = 1.0$. The SCFT potentials corresponding to the LPE monomers, $w_{LPE}(r)$, are used to effect Monte Carlo simulations of semi-flexible chains as described in the next section.

2.2 Monte Carlo simulation of the LPE chains

As discussed earlier, Monte Carlo simulations are used in our work as a means to access the conformational features of the LPE chains. In our MC simulations, we simulate worm-like chains (Kratky–Porod model)[40] that interact only with the field, $w_{LPE}(r)$ (obtained from SCFT calculations). The latter incorporates the effects of the electrostatic and steric interactions of the LPEs with the dendrimer. The semi-flexible chain consists of $N_{LPE} + 1$ monomers connected by N_{LPE} bonds of fixed length b, and the energy of the system is given by:

$$\frac{\mathscr{F}}{k_B T} = \sum_{i=1}^{n_{LPE}} \sum_{s=1}^{N_{LPE}} \left[\frac{\lambda}{b}(1 - \cos(\theta_{i,s})) + b w_{LPE}(\boldsymbol{r}_i(s)) \right], \tag{6}$$

where λ is the persistence length of chain, $\boldsymbol{r}_i(s)$ denotes the position of s^{th} monomer in the i^{th} chain, $\theta_{i,s}$ is the angle between bonds sharing a vertex at $\boldsymbol{r}_i(s)$, n_{LPE} is the total number of polyelectrolyte chains in the system, k_B is Boltzmann's constant, and T is temperature. The MC simulations are performed in canonical ensemble of 1000 chains ($n_{LPE} = 1000$). The polyelectrolyte chains are placed at random in a simulation box of length equal to 100 bond length units. The radial field, $w_{LPE}(r)$ (with the dendrimer at $r = 0$), from the SCFT simulations is superimposed onto the center of the simulation box. The chain conformations are sampled by employing a combination of crank-shaft rotation, slithering snake, and pivoting moves.[55] Metropolis criterion based on the energetic differences is used to accept or reject the proposed conformations.[56] Each MC cycle consists of one attempt of crank-shaft rotation per monomer and an attempt of both a pivot and slithering snake move per chain. The pivot and slithering snake steps are global moves, which help to enhance the diffusion of the LPE chains.

In the MC simulations, the system is first equilibrated for 3×10^6 MC cycles and then various structural quantities are averaged each 100 MC cycles for 3×10^6 more MC cycles. The averaged quantities include radially averaged radius of gyration, the center of mass density of polyelectrolyte chains, and loop/tail distributions (*cf.* Fig. 1b for the definitions of loops, tails, and trains).

2.3 Parameters

In this study, we fixed the generation number, functionality, and spacer length of the dendrimer to be $g = 3, f = 3$, and $n = 5$ respectively. In order to examine the effects of grafting length, we varied the grafting length from $N_G = 0$ to $N_G = 30$. In each of our calculations, we fixed the average dendrimer monomer fraction, $\bar{\varphi}_P \equiv M/(V\rho_0)$, to be 2.09×10^{-5}, which corresponds to a single non-grafted ($N_G = 0$) dendrimer in a simulation cell of 75 R_g (where $R_g = \sqrt{Na^2/6}$ and $N = (g+1)n + N_G$ is the contour length from the center of the dendrimer to the edge of the grafted chain). We fixed the fraction of dendrimer monomers that are capable of charge dissociation at $\alpha_P = 0.5$. For our simulations, we choose an arbitrary value of $pK_{b,P} = 5.0$, but express our results in terms of $pOH - pK_{b,P}$. Unless otherwise noted, the $pK_{b,P}$ of the dendrimer monomers matches the solution pOH in our simulations.

We note that fixing α_P does not necessarily fix the total charge carried by the dendrimer. Indeed, the local fraction of dissociated monomers in the dendrimer, $\alpha(r)$, is inhomogeneous and given by

$$\alpha(r) = \frac{1}{1 + 10^{pK_{b,P} - pOH} \exp(-z_{OH^-}\Phi(r))}, \tag{7}$$

where z_{OH^-} is the valency of the OH^- ions and $\Phi(r)$ is the non-dimensional electrostatic potential (see Appendix). From eqn

(7), we see that the local dissociation depends on the local electrostatic potential, $\Phi(r)$, and the difference in dendrimer $pK_{b,P}$ and solution pOH. The high degree of branching associated with polyelectrolyte dendrimers results in a high density of charged monomers within the dendrimer and makes localization of the OH^- counterions energetically favorable at equilibrium.[39,50–54,57,58] Increasing the local concentration of OH^- ions results in a decreased probability of monomer dissociation through eqn (4). Since the local probability of monomer dissociation varies in space, we also calculate the average dissociated fraction of the dendrimer, $\bar{\alpha}$, which is given as:

$$\bar{\alpha} = \frac{\alpha_P \int_0^\infty dr r^2 \alpha(r) \varphi_P(r)}{\int_0^\infty dr r^2 \varphi_P(r)}. \quad (8)$$

Based on the above discussion, we expect the average dissociation ($\bar{\alpha}$) to be always less than the fraction of monomers that can participate in the charge dissociation reaction ($\alpha_P \alpha_b$).[39,57,58]

We fix the LPE chain length to be $N_{LPE} = 50$ and the fraction of charged LPE monomers, α_{LPE}, to be 1.0. The non-dimensional persistence length (PL) of the LPE chains, $\mu = PL/(N_{LPE}a)$ (where a is the Kuhn segment length and is assumed to be 0.7 nm, the Bjerrum length of water), is varied from $\mu = 0.02$ to $\mu = 0.4$. We modeled the LPE molecules in a grand canonical framework and fixed their bulk density to be $\varphi_{LPE,b} = 0.0001$. The solution screening length, κ^{-1}, is given by $\kappa^2 = 4\pi l_B \sum_i c_i z_i^2$ (where c_i is the concentration of the free ion and LPE species) and was fixed to be $3a$. To maintain a fixed screening length under varying pOH conditions, we adjusted the bulk salt concentration of the solution appropriately with changes in pOH.

3 Results

Below we discuss results displaying the effects of neutral dendrimer grafts, LPE stiffness, and solution pOH on the conformations and structure of dendrimer–LPE complexes. Specifically, we seek to identify the influence of different parameters upon the following characteristics:

3.1 The amount and conformations of complexed LPEs

A key quantity characterizing the efficacy of dendrimers in gene therapy applications is the exposure of the complexed LPEs to solvent medium and the degradative enzymes present therein. To quantify such features, we first define the radius of the grafted dendrimer, R_{PG} as:

$$R^2_{PG} = \frac{\int_0^\infty dr r^4 (\varphi_P(r) + \varphi_G(r))}{\int_0^\infty dr r^2 (\varphi_P(r) + \varphi_G(r))}, \quad (9)$$

where $\varphi_P(r)$ and $\varphi_G(r)$ are the respective volume fraction profiles of the dendrimer and graft portions of the grafted dendrimer. Subsequently, we identify complexed LPEs as those having at least one of their monomers residing within R_{PG}.

For complexed chains, we quantify their "exposure" through the distribution of loops and tails. Loops and tails refer to segments of adsorbed LPE chains which lie outside R_{PG}. For loops, *both* ends of the loop connect to monomers which lie within R_{PG}. In contrast for a tail, *only one* of the tail monomers is attached to a LPE monomer residing within R_{PG} (*cf.* Fig. 1b for a pictorial representation of loops, tails, and trains). Using our MC simulations, we quantify the fraction of adsorbed chains that reside in loops and tails (denoted as f_{loop} and f_{tail} respectively) and the average length of loops and tails (denoted as $\langle N_{loop} \rangle$ and $\langle N_{tail} \rangle$ respectively).

3.2 Charge of the resulting dendriplex

Typically, the positive charge carried by the cationic delivery vectors leads to their binding with negatively charged genetic material. The expectation is that the complex will possess a net positive charge which will facilitate an energetically favorable interaction with the negatively charged cell membranes. In this context, it is of immense interest to understand the influence of different physical parameters upon the overall charge of the complex. In our work, we quantify the effective charge of the dendrimer complex through a local quantity, $Q(r)$, defined as:

$$Q(r) = \int_0^r dr' 4\pi \rho_0 r'^2 \varphi_e(r'), \quad (10)$$

where $\rho_0 \varphi_e(r')$ is the local density of charge. Eqn (10) quantifies the total charge contained in a sphere of radius r, with the center of the sphere fixed at $r = 0$. We use the behavior of $Q(r)$ to understand the effects of dendrimer and LPE parameters on the resulting charge of the complex.

3.3 Binding strength between the dendrimer and LPE molecules

After successful delivery of genetic material to the cell has occurred, the dendrimer and NA material must dissociate. To quantify the role of different physical parameters upon the ease of dissociation, we quantify the binding strength through the potential of mean force (PMF), $w_{PMF}(r)$, for the interactions between the LPE and dendrimer. The potential of mean force quantifies the difference in free energy of a dendrimer and LPE whose COMs are separated by a distance r relative to infinite dendrimer–LPE separation. Strictly speaking, $w_{PMF}(r)$ requires calculation of free energies for a dendrimer and LPE at a fixed distance r from the core of the dendrimer. However, we use a more approximate framework wherein the center of mass density of LPEs obtained from our MC simulations, $\rho_{COM}(r)$, is used to deduce $w_{PMF}(r)$ through:

$$w_{PMF}(r) \simeq -k_B T(\ln[\rho_{COM}(r)] - \ln[\rho_{COM,b}]), \quad (11)$$

where $\rho_{COM}(r)$ and $\rho_{COM,b}$ are the local COM and bulk concentration COM densities respectively. The above expression is expected to be valid for dilute concentrations of LPE and does not account for the deformation of the dendrimer arising from fixing the LPE at a distance r.

In presenting our results, we first present the SCFT results characterizing the influence of the different parameters upon the local volume fractions of the dendrimer and LPE molecules and the orientational order of the LPE molecules. We then discuss the results for the above quantities of interest, *viz.* (i) loop and tail distributions, (ii) charge of the dendriplex, and (iii) dendrimer–LPE potential of mean force.

3.4 Effect of persistence length on LPE complexation

The binding mechanism between charged dendrimers and linear polyelectrolytes has been largely attributed to the electrostatic attraction between the charged dendrimer monomers and LPE molecules.[18,19,22] Since dendrimers have been shown to effectively bind to both single and double stranded DNA and RNA molecules,[8–13] it is of interest to gain fundamental insight into the effect of LPE stiffness upon dendrimer–LPE binding affinities. Previous works by both Tian and Ma[29] and Klos and Sommer[31] have addressed the effects of LPE stiffness upon the properties of complexed dendrimers. Below we present results which complement the results presented in their works, and also make comparisons where appropriate.

Dendrimer–LPE conformations. We first consider the situation of a non-grafted $g = 3$ dendrimer with LPEs of different persistence lengths (μ). Fig. 2a displays the volume fraction profiles of the dendrimer monomers not in the presence of LPE molecules (dashed violet line) and in the presence of LPEs having persistence lengths of $\mu = 0.02$, 0.1, 0.2, and 0.4. Consistent with results of earlier works,[39,57–59] the dendrimer displays a dense core conformation, with a maximum in the monomer density near the center followed by a monotonic decay with increasing r. Interestingly, we observe in Fig. 2a that the dendrimers participating in complexation with the stiffer LPE molecules have more open conformations as compared to the case involving more flexible LPE chains. Furthermore, we observe that the dendrimers not in the presence of LPEs have the most open conformations. Such a behavior can be rationalized through examination of the corresponding LPE volume fraction profiles, which are displayed in Fig. 2b. There we observe that the local density of LPE monomers within the dendrimer decreases with increasing μ, whereas the extent of the LPE density tails increases with μ. Such a lowering of the LPE monomer density within the dendrimer molecule results in a higher net positive charge density and consequently results in a more open conformation of the dendrimer due to the resulting electrostatic repulsions.

Loop and tail statistics. To further understand the observed behavior in the LPE density profiles, in Fig. 3 we display the effect of persistence length on the statistics of the loops and tails. Explicitly, Fig. 3a displays the fraction of complexed LPE chain monomers which exist as loops (f_{loop}) and tails (f_{tail}). We observe that f_{loop} decreases with increasing μ, whereas f_{tail} is seen to increase with μ. Further, we see that f_{tail} is much more sensitive to μ than f_{loop}, suggesting that increasing the persistence lengths of the LPE results in a large fraction of the LPE monomers being pushed outside of the dendrimer as tails. These results serve to explain our observations from Fig. 2b, which displayed a decrease in local LPE volume fraction within the dendrimer with increasing μ.

To provide a more pictorial depiction of the trends displayed in Fig. 3a, we display snapshots of $\mu = 0.02$ and $\mu = 0.4$ LPE molecules complexed with non-grafted $g = 3$ dendrimers in Fig. 4a and b respectively. The flexible chains (Fig. 4a) are seen to exhibit short tails and a significant number of loops, with a large number of monomers residing within the dendrimer due to the coiled conformations of the LPE chains. In contrast, the stiff LPE chains (Fig. 4b) have long protruding tails (with no loops observed in the displayed snapshots). Furthermore, the flexible chains have a high number of monomers residing within the dendrimer (Fig. 2b), while the stiff chains have only a relatively straight train of monomers residing within the dendrimer.

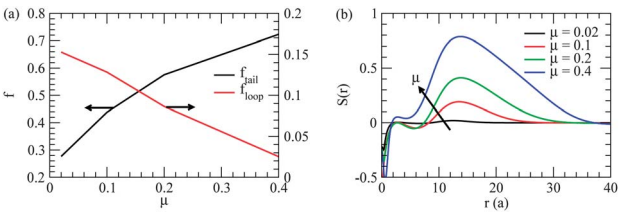

Fig. 3 (a) Effect of PL on the fraction of dendriplex loops and tails; (b) Effect of persistence length on the order parameter, $S(r)$.

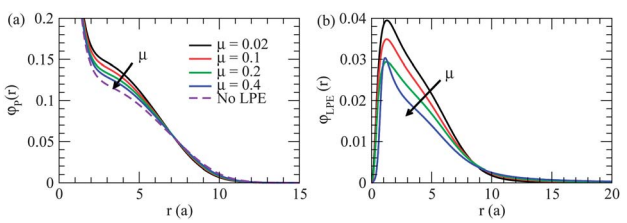

Fig. 2 (a) Volume fraction profiles of $g = 3$ non-grafted dendrimer monomers complexed with $N_{LPE} = 50$ polyelectrolyte molecules of varying persistence lengths. (b) Effect of persistence length on the LPE monomer volume fraction profiles.

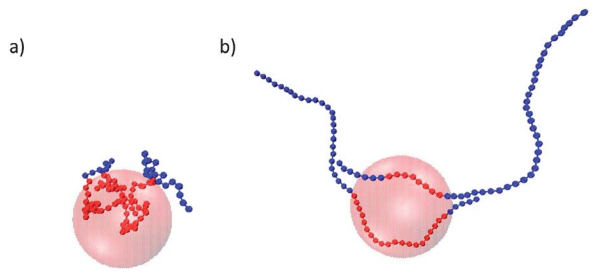

Fig. 4 Snapshots of $\mu = 0.02$ (a) and $\mu = 0.4$ (b) LPE chains complexed with a $g = 3$ dendrimer (represented as red sphere). The LPEs are color coded such that the monomers residing within the dendrimer sphere are depicted in red while the monomers outside of the dendrimer are indicated in blue.

To clarify further the above-noted differences in the conformations of the stiff and flexible LPEs within the LPE–dendrimer complex, we display the spatially dependent order parameter, $S(r)$, for different values of μ in Fig. 3b. For all cases, we observe a non-monotonic behavior of the order parameter as a function of distance from the center of the dendrimer. We note that the negative values of $S(r)$ correspond to situations where the LPE molecules adopt conformations which are perpendicularly oriented to the radial vector, whereas positive order parameter values correspond to the situation wherein the axes of the LPE molecule is aligned on an average with the radial vector. We generally notice negative or small positive values for the order parameter near the core of the dendrimer molecule, which can be explained by noting that near the dendrimer core, there is a high density of dendrimer monomers, which creates steric repulsion between the dendrimer and LPE monomers. Since the LPE monomers are not able to penetrate the center of the dendrimer core, they reside near and bend around the core, resulting in a perpendicular orientation of the LPE to the radial vector. Moving outward from the core, we notice a rather steep increase in the order parameter until it reaches a maximum value, consistent with the radial alignment of the LPE monomers. As μ increases, we begin to notice an increase in the maxima and distribution widths of $S(r)$, which is indicative of the protrusion of long tails outward from the dendrimer center for stiff chains, in agreement with the snapshot of Fig. 4b. In contrast, the results of Fig. 3b suggest that the flexible chains reside in conformations that have little ordering ($S \approx 0$), corresponding to an almost globular conformation (*cf.* Fig. 4a).

In sum, the above results for the volume fraction, loop and tail, and order parameter data display that increasing LPE stiffness results in the enhancement of exposed LPE material. Physically, this phenomena results from the competition between electrostatic and bending energies.[29,31] Indeed, on the one hand, electrostatic interactions favor the chains to maximize their contact with the dendrimer monomers. However, due to the spherical shape and small spatial dimensions of the dendrimers, assuming a LPE conformation which maximizes contact with the dendrimer requires a highly coiled LPE conformation. Increasing the LPE persistence length results in a higher bending energy, which suppresses the chain's ability to assume a highly coiled conformations. This in turn results in longer tail formation and reduced LPE localization within the dendrimer.

Dendriplex charge. As discussed previously, the overall charge of the dendrimer complex is hypothesized to play an important role in the cellular internalization of dendriplexes.[1,2,4–10,12,21] Thus, it is of interest to examine the effect of persistence length of the LPE on the charge of the resulting complex. We note that dendrimers are often composed of weakly basic amine groups, in which the local charge dissociation is sensitive to the local concentration of counterions.[39,53,57,58] In the absence of LPEs, the high density of charged monomers carried by the dendrimer molecules correspondingly results in significant counterion localization. In the presence of LPE molecules, which by themselves also carry a large number of negatively charged monomers, we expect that complexation with the dendrimer would affect the local density of counterions and thereby modulate the dissociation of the dendrimer monomers.

In Fig. 5a, we display the effect of LPE persistence length on the local dendrimer charge dissociation profiles, $\alpha(r)$, and the OH^- volume fraction profiles, φ_{OH^-} (inset). Consistent with our above expectations, we observe that the addition of LPE molecules to the system results in a significant reduction in the amount of OH^- ions within the dendrimer, which in turn enhances the local probability of charge dissociation in the dendrimer monomers. More quantitatively, we found that the bare dendrimers (in the absence of LPE molecules) carried charge fractions of $\bar{\alpha} = 0.166$ (eqn (8)), whereas, dendrimers in the presence of $\mu = 0.4$ LPE molecules carried a charge fraction of $\bar{\alpha} = 0.211$. We note that the reduction in counterion localization within dendrimers upon dendrimer–LPE complexation has been observed previously in the simulations of Tian and Ma.[29] However, their study did not consider the weakly basic nature of dendrimer molecules and hence could not account for changes in the dissociation of the dendrimer monomers. Thus, the inclusion of LPE molecules is seen to have a significant effect upon the overall dissociation of weakly basic dendrimers.

Relative to the effects arising from the addition of LPE chains to the system, we notice that modulating the LPE stiffness has a much smaller impact on the charge dissociation of the dendrimer. In general, we observe that the amount of counterion localization within the dendrimer decreases with decreasing μ,

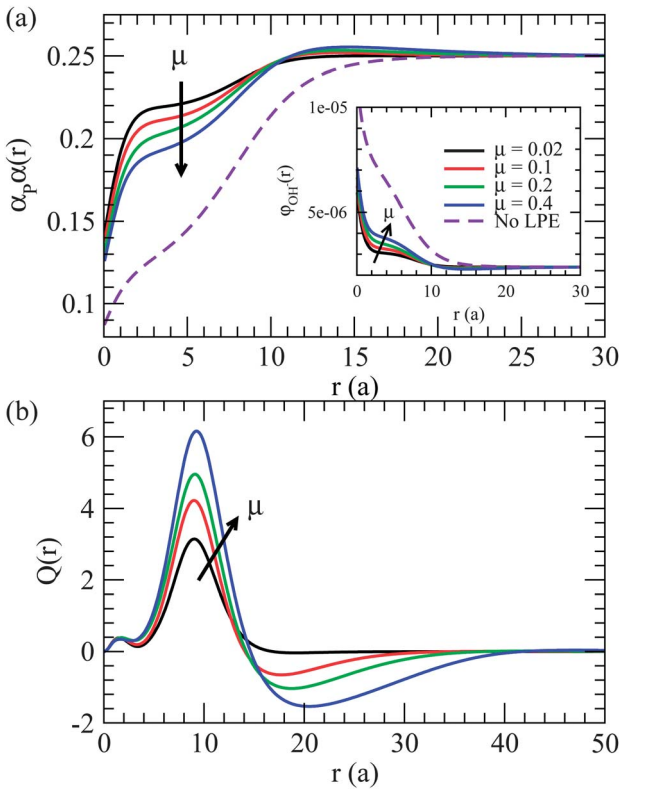

Fig. 5 (a) The effect of PL on the local probability of dendrimer charge dissociation, $\alpha_P\alpha(r)$. The inset displays the corresponding OH^- counterion density profiles. (b) The effect of PL on the effective charge as a function of r.

which in turn enhances the local probability of monomer dissociation. Physically, such results can be understood to be a consequence of the decreased localization of stiff LPEs within the dendrimer as compared to the flexible LPE chains. Interestingly, we notice a slight depletion of OH^- ions just outside of the dendrimer periphery for the $\mu = 0.4$ LPEs. We attribute this phenomena to the presence of the long negative tails of LPE protruding from the dendriplex, which act to locally deplete negatively charged ions.

In order to examine the effect of persistence length of the LPEs upon the charge of the resulting complex, we present $Q(r)$ (eqn (10)) in Fig. 5b. Overall, as we move out from the core of the dendrimer, we observe an increase in $Q(r)$ until it reaches a maxima around $r = 9a$ (which corresponds to $1.4R_{PG}$). Subsequently, $Q(r)$ is seen to drop and become negative at larger r before becoming zero (*i.e.* neutral) for large r. To understand these results, we note that the core of the dendrimer–LPE complex is primarily populated by the positively charged dendrimer monomers (*cf.* Fig. 2a), and hence the core region of the dendrimer–LPE complex is expected to be positively charged. The negatively charged LPE monomers are seen to reside in the region exterior to the dense core. The latter neutralizes the charges of the dendrimer monomers and leads to the decrease in $Q(r)$. The outer fringes of the complex are primarily populated by the tails of the negatively charged LPE monomers, which explains the dip in $Q(r)$ to negative values. Interestingly, we notice that the magnitudes of both the maxima within the dendrimer and the minima outside of the dendrimer increases with increasing μ. These dependencies on μ can be rationalized through the $\varphi_{LPE}(r)$ plots in Fig. 2b, which show a decrease in local LPE concentration within the dendrimer and a correspondingly longer tail.

In their recent work, Tian and Ma noticed a positive gain in dendriplex charge as LPE stiffness was increased,[29] a trend which qualitatively matches our above results. Likewise, Klos and Sommer noticed a decrease in the number of condensed LPE monomers as the stiffness was increased, which would correspond to a higher positive charge within the dendrimer.[31]

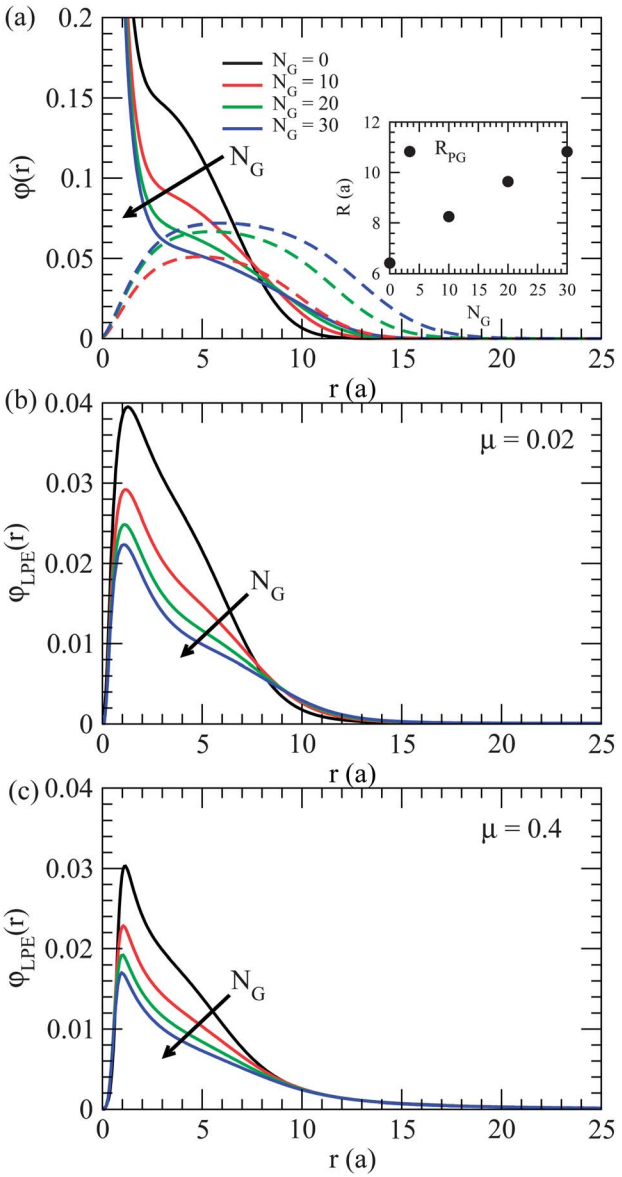

Fig. 6 (a) Volume fraction profiles of $g = 3$ dendrimers (solid lines) and their respective grafted monomers (dashed lines) complexed with $\mu = 0.02$, $N_{LPE} = 50$ LPE molecules. The inset displays the R_{PG} values of the dendrimers as a function of N_G. Volume fraction profiles of LPEs having $\mu = 0.02$ (b) and $\mu = 0.4$ (c) complexed with dendrimers of varying N_G.

3.5 Effect of grafting length on LPE complexation

In the previous section, we witnessed that increasing the LPE stiffness resulted in an increased LPE exposure through the presence of long tails. Correspondingly, we witnessed the presence of a negatively charged region outside of the dendrimer molecule, which might affect interaction with the negatively charged cellular membrane. Because the use of grafted dendrimers has been proposed as an alternative to non-grafted dendrimers, below we presents results illustrating the influence of grafts on LPE exposure, dendriplex charge, and dendrimer–LPE binding strengths.

Dendrimer–LPE conformations. We begin by discussing the influence of grafts upon the dendrimer conformations. Fig. 6a displays the density profiles of grafted dendrimers for varying values of N_G in the presence of flexible LPEs ($\mu = 0.02$). We observe that increasing N_G lowers the dendrimer monomer densities near the core and results in an extended tail. Correspondingly, the penetration of grafted chains within the dendrimer and the overall extent of the grafts are seen to increase with N_G. As a result, the size of the dendrimer molecule (R_{PG}) increases with N_G (displayed as a function of N_G in the inset).[58] Since adding grafts to the dendrimer is seen to result in significant conformational changes of the dendrimers, it can be expected that such changes would also affect the way the LPE molecules complex with the dendrimer. Fig. 6b and c show the effect of N_G on the local concentration of LPE monomers within the dendrimer for the cases of LPEs with $\mu = 0.02$ and 0.4 respectively. The general behavior of the LPE volume fraction profiles mirrors the non-monotonic trends of the LPE volume fraction profiles observed in Fig. 2b. For both types of LPE molecules, we observe that increasing N_G results in a local

decrease in the density of LPE monomers near the dendrimer core. The N_G dependence of the LPE density profiles and conformations can be attributed to two factors: (i) the increased segregation of the charged dendrimer monomers towards the periphery seen in Fig. 6a, which results in an attraction of negatively charged LPEs to such regions, and (ii) the enhanced steric repulsions arsing from the presence of grafted polymer monomers near the dendrimer center.

Loop and tail formation. In order to quantify the exposure of the LPE molecules in the complexes with grafted dendrimers, Fig. 7a–d display both the fraction and average lengths of loops and tails of the complexed LPEs. Both Fig. 7a and b show that the fraction of material existing in loops and tails decreases with increasing grafting length, suggesting that the grafted dendrimers are better capable of shielding the LPE molecules from the surrounding medium. Correspondingly, in Fig. 7c and d we observe a monotonic decrease in the average lengths of loops and tails as N_G increases. The relative decrease in the amount of material existing in loops and tails is seen to be much higher for the flexible chains. Flexible chains have highly coiled conformations, allowing them to more easily reside within the dendrimer. The presence of grafts provides a larger *volume* in which the flexible LPEs may reside, which in turn reduces the probability that portions of adsorbed chain monomers may be exposed. On the other hand, the stiff LPE chains have much more linear conformations, and thus the increase in the size of the dendrimer only provides a larger *radius* over which the LPEs can be located. Hence, the changes in f_{loop} and f_{tail} are relatively smaller for persistent chains. In support of the preceding argument, we observe that f_{tail} in Fig. 7b decreases linearly with N_G, which mirrors the near linear increase in R_{PG} with respect to N_G displayed in the inset of Fig. 6a. Overall, the above results suggest that the addition of grafts to the dendrimer results in a significant impact on the exposure of complexed LPEs. Such results are consistent with recent observations reported in Fant *et al.*, where PEGylated PAMAM dendrimers were seen to better protect plasmid DNA from degradative serum nucleases than corresponding acetylated PAMAM dendrimers.[9]

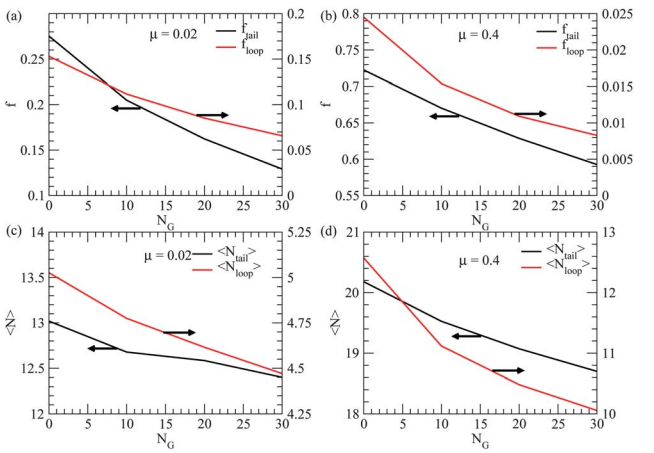

Fig. 7 (a and b) Effect of N_G on f_{tail} and f_{loop} for $\mu = 0.02$ (a) and $\mu = 0.4$ (b). (c and d) Effect of N_G on $\langle N_{tail}\rangle$ and $\langle N_{loop}\rangle$ for $\mu = 0.02$ (c) and $\mu = 0.4$ (d).

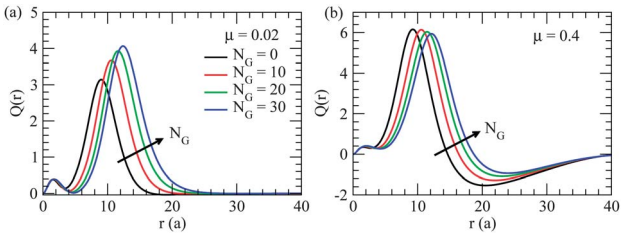

Fig. 8 Effect of N_G on the integrated charge distributions, $Q(r)$, for $\mu = 0.02$ (a) and $\mu = 0.4$ (b).

Dendriplex charge. As observed in the previous section, the presence of LPE molecules, especially the case of stiff LPEs, resulted in significant modulation in overall charge of the dendrimer molecules (*cf.* Fig. 5). The influence of grafts on such characteristics are displayed in Fig. 8. Overall, the qualitative shape of the profiles is seen to match those from Fig. 5b. However, we do notice that increasing N_G has the overall effect of shifting the global $Q(r)$ maxima to further radial values, an effect which can be attributed to the graft-induced outward segregation of the charged dendrimer monomers. Interestingly, the maximum values of $Q(r)$ are seen to increase with N_G for complexes with flexible LPE chains. Such trends can be rationalized from the results displayed in Fig. 6, wherein it is seen that the addition of grafts to the dendrimer reduces the extent to which the LPE chains penetrate inside of the dendrimer. In contrast, we observe that for stiff LPEs, increasing N_G results in a slight reduction in the $Q(r)$ maxima. Since the addition of grafts moves the charged dendrimer monomers outwards, increasing N_G enhances contact between the stiff LPEs and charged dendrimer monomers, thus allowing LPE chains to better compensate the charge of the dendrimer monomers. Due to such compensation effects, we observe that the valley in $Q(r)$ becomes less significant with an increase in N_G. We note that in the gene silencing studies of Tang *et al.*,[12] the addition of grafts to $g = 5$ and $g = 6$ dendrimers was shown to reduce the corresponding zeta potentials (from 34.5 to 26.9 for $g = 5$ dendrimers, and from 33.6 to 27.9 for $g = 6$ dendrimers), suggesting an overall reduction the effective charge of the dendrimers. This trend is in qualitative agreement with the results from Fig. 8b.

Dendrimer–LPE PMF. To quantify the influence of grafts upon the binding strength between LPEs and dendrimers, in Fig. 9a and b we display the PMFs for LPE molecules ($\mu = 0.02$ (a) and 0.4 (b)) interacting with dendrimers of varying N_G values.

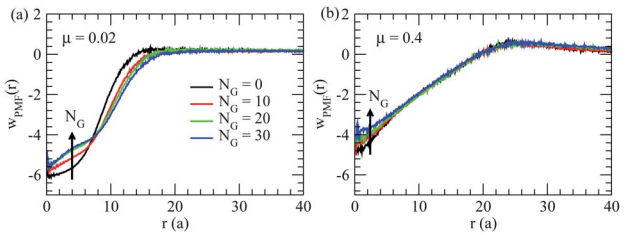

Fig. 9 Effect of N_G on the potential of mean force profiles for $\mu = 0.02$ (a) and $\mu = 0.4$ (b) LPE molecules.

In general, we notice that the more flexible chains exhibit a deeper potential well and hence a strong binding to dendrimers of a given grafting length. For the flexible chains, we notice that increasing grafting length reduces the magnitude of the potential well depth while increasing its width. Physically, we attribute this phenomena to both the enhancement of steric repulsions between the conjugated dendrimer and LPE monomers and the accompanying localization of charged dendrimer monomers to further radial values. Interestingly for the stiff chains, the effect of N_G on the dendrimer–LPE PMF profiles are seen to be minimal, suggesting that the binding between the dendrimer and stiff LPE molecules is not affected by the addition of grafts. As discussed in the context of $Q(r)$ profiles, increasing N_G of the stiff LPE dendriplexes results in two competing effects, *viz.*, the steric interactions induced reduced localization of LPE monomers and the enhanced number of electrostatically favorable contacts resulting from the increase in the radius of the dendrimer. We speculate that two preceding effects compensate and lead to a weak LPE–dendrimer binding strength dependence on dendrimer grafting length for stiffer chains.

In conclusion, we have shown that the addition of grafts to dendriplexes reduces the amount of exposed LPE material, an effect which likely which is beneficial from the perspective of trying to reduce degradation of genetic material by serum nucleases. For stiff LPE molecules, we notice that the addition of grafts reduces the amount of overcharging (negative $Q(r)$ values), while not having a strong affect on the strength of binding between the dendrimer. In contrast, increasing the grafting length of dendriplexes comprised of flexible LPEs results in a reduction in the binding strength, with no overcharging observed.

3.6 Effect of pOH on complexation

Transport of the dendriplex through the cellular membrane requires endosomal escape, a process triggered through a decrease in pH within the endosome. Below, we present results quantifying the effect of solution pOH on the dendrimer–LPE binding strengths and the overall dendriplex charge. The former quantifies the influence of changing solution conditions on the ease of release of LPEs, whereas the latter is expected to have implications for the interaction of the dendriplexes with the endosomal membrane.

Dendrimer–LPE PMF. Since electrostatic interactions have been shown to be the main mechanism through which dendrimers bind to LPEs,[18,19,22] in Fig. 10a we first present results illustrating the influence of pOH upon the charged monomers of the dendrimers. Explicitly, Fig. 10a depicts the volume fraction profiles of the $N_G = 30$ charged dendrimer monomers ($\alpha_P\alpha(r)\varphi_{LPE}(r)$), for different pOH conditions. Consistent with physical expectations (eqn (3)), we observe that increasing the solution pOH results in higher densities of charged monomers, which extend over a larger region of space.

It is expected that the above pOH induced enhancement on the dendrimer charge will have a significant effect on the conformation and binding of the LPE molecules. In Fig. 10b, we

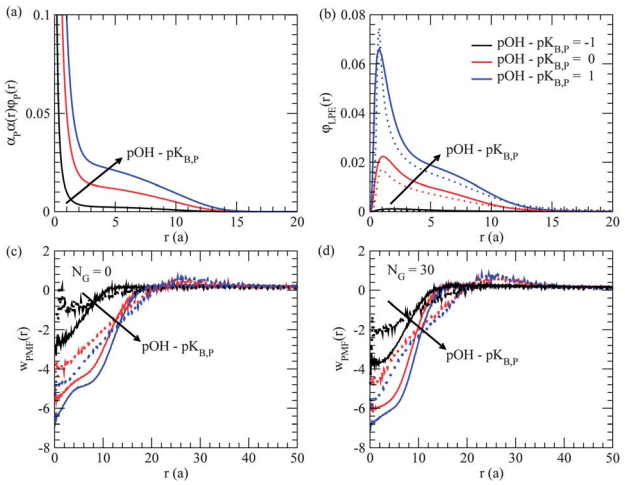

Fig. 10 (a) Density profiles of charged dendrimer monomers for a $N_G = 30$, $g = 3$ dendrimer complexed with $\mu = 0.02$ LPE molecules. (b) LPE volume fraction profiles (solid lines for $\mu = 0.02$, dotted lines for $\mu = 0.4$) that are complexed with $N_G = 30$, $g = 3$ dendrimers for varying values of pOH $- pK_{b,P}$. Effect of pOH on the PMF profiles of $\mu = 0.02$ (solid lines) $\mu = 0.4$ (dotted lines) LPEs in the presence of $N_G = 0$ (c) and $N_G = 30$ (d) dendrimers.

display LPE density profiles for varying values of pOH. The LPE profiles are seen to maintain the general shapes discussed in the context of Fig. 2b, 6b and c. However, we observe that increasing the pOH of the solution results in an enhancement of LPE monomers inside the dendrimer core and in the outer shell. These effects can be attributed to the enhancement of dendrimer monomer charge dissociation seen in Fig. 10a. Moreover, in agreement with our previous observations, we see that increasing the stiffness of the LPE chains decreases the overall density of the LPE chains, but in turn extends the LPE density tail.

In Fig. 10c we display the effect of pOH upon PMFs for non-grafted dendrimer–LPE systems. We observe that increasing the solution pOH results in an increase in the magnitude of the strength of interaction between the dendrimer and the LPEs. In comparing flexible and stiff chains we observe that the stiffer chains display lower strengths of association, which is consistent with our discussion in the previous section. In comparing the grafted and non-grafted complexes (*cf.* Fig. 10d), we again observe (see Fig. 8) that the grafts influence the binding of flexible chains compared to stiff LPEs. Overall, the above results indicate that a low pH environment, *e.g.* inside the lysosome, is expected to lead to strong binding between dendrimer and DNA molecules. Hence, dissociation of the dendrimer–LPE complexes are more likely to occur within the cytoplasm as compared to the endosome.

Dendriplex charge. In Fig. 11, we display $Q(r)$ of the dendriplexes for varying solution pOH conditions. We observe that increasing the solution pOH results in a higher net charge carried by the dendrimers and a higher level of overcharging of the dendrimer for the stiff LPEs. The increase in the maxima in $Q(r)$ can be attributed to the increase in dendrimer charge that accompanies the increase in solution pOH. In qualitative agreement with the results in Fig. 5b (and the discussions

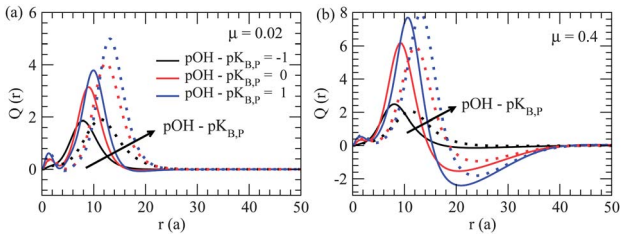

Fig. 11 Effective charge profiles, $Q(r)$, of dendriplexes for varying values of pOH − $pK_{b,P}$. The solid lines correspond to the non-grafted dendrimers and the dotted lines correspond to the case of grafted dendrimers with $N_G = 30$.

therein), we observe that for a given pOH increasing μ results in an enhancement of the maxima in $Q(r)$. Likewise, we observe that increasing the dendrimer grafting length reduces the amount of "overcharging" witnessed for the stiff LPEs (*cf.* Fig. 8). For both the stiff and flexible LPE complexes, we observe that an increase in pOH not only enhances the binding between the dendrimer and LPE molecules, but also increases the overall positive charge of dendriplex. The latter may prove beneficial for disruption of the endosome capsule, a process which needs to occur before the onset of lysosomal degradation.

4 Summary

In this article, we presented results of a study using a hybrid methodology of SCFT calculations and MC simulations to understand the influence of chain stiffness, neutral dendrimer grafts, and solution pOH upon the complexation between weakly basic polyelectrolyte dendrimers and linear polyelectrolyte molecules. We observed that an increase in the LPE stiffness resulted in a reduction in the localization of LPE chains within the dendrimer molecule and, in turn, an increased positive charge within the dendrimer. The complexation stiff LPEs results in the protrusion of long tails and a negatively charged shell outside the dendrimer. The presence of LPE molecules within the system was also seen to result in a significant decrease in the amount of condensed counterions, which in turn enhanced the amount of dendrimer monomers that were charged, a synergistic effect which enhanced the binding between the dendrimer and LPE. This phenomena was seen to be most prominent for the highly flexible LPE chains. From our MC simulations, we are able to quantify the PMF between the dendrimer and LPE molecules, and observed that increasing LPE stiffness resulted in a decrease in binding strength.

The addition of grafts to the dendrimer was seen to affect not only the dendrimer conformations, but also the binding between the dendrimer and LPE molecules. Increasing dendrimer grafting length resulted in decreased localization within the dendrimer for both flexible and stiff chains. For the flexible LPEs, we observed that increasing the grafting length resulted in more positive charge being carried within the dendrimer molecule, an effect which was attributed to the increase in exclusion of LPE monomers from the dendrimer due to steric repulsions. In contrast, for the stiffer LPE chains, we noticed a slight decrease in the positive charge within the dendrimer with increasing grafting length. Although increasing grafting length resulted in a reduction in LPE monomer density near the dendrimer center, the increased stretching of the dendrimer branches in turn enhances the contact between the charged dendrimer and LPE monomers. These two competing effects ultimately led to a reduction in the positive charge carried within the dendrimer and the negative charge in the shell outside of the dendrimer. Lastly, we studied the effect of solution pOH on the binding between the dendrimer and LPE molecules. Here we observed that increasing pOH (decreasing pH) results in enhanced binding between the LPE and dendrimer molecules.

This paper, along with previous works,[17–20,22–31] has provided insights on physics relevant to dendrimer–LPE complexation in the framework of a single dendrimer in the presence of LPE molecules. Although it is valuable to understand how dendrimer and LPE parameters affect the resulting dendriplex charge, physically relevant dendriplexes have length scales that exceed the dimensions of a single dendrimer and DNA/RNA molecule.[8,12,13] Indeed, simulations have examined the binding between a single LPE molecule and multiple dendrimers.[19,28] In future works, we plan to extend the present framework to understand the role of multi-body dendrimer LPE interactions on the formation of dendrimer–LPE complexes to obtain a physically accurate picture.

A Appendix

In this appendix, we describe the model details and the equations accompanying our coarse-grained mean-field modeling of the dendrimer-graft-LPE system. Much of the details of the formalism are identical to that employed and elaborated in our earlier works.[39,57,58]

A.1 Free energy terms

We employ a semi-grand canonical framework to describe the free energy of our system, and we solve it within a mean field approximation.[40] In this framework, the free energy $\mathscr{F}$ can identified as:[50]

$$\mathscr{F} = \mathscr{F}_{\mathrm{mix}} + \mathscr{F}_{\mathrm{elec}} + \mathscr{F}_{\mathrm{comp}} + \mathscr{F}_{\mathrm{conf}}. \tag{12}$$

The first term,

$$\begin{aligned}\beta\mathscr{F}_{\mathrm{mix}} = &\int \mathrm{d}\boldsymbol{r} \sum_k \left\{\varphi_k(\boldsymbol{r})\left[\ln\varphi_k(\boldsymbol{r}) - 1 + \beta\gamma_k^{\mathrm{o}}\right]\right\} \\ &+ \int \mathrm{d}\boldsymbol{r}\alpha_{\mathrm{P}}\varphi_{\mathrm{P}}(\boldsymbol{r})\alpha(\boldsymbol{r})\left(\ln(\alpha(\boldsymbol{r})) + \beta\gamma_{\mathrm{PH}^+}^{\mathrm{o}}\right) \\ &+ \int \mathrm{d}\boldsymbol{r}\alpha_{\mathrm{P}}\varphi_{\mathrm{P}}(\boldsymbol{r})(1-\alpha(\boldsymbol{r}))\left(\ln(1-\alpha(\boldsymbol{r})) + \beta\gamma_{\mathrm{P}}^{\mathrm{o}}\right),\end{aligned} \tag{13}$$

represents the mixing entropies of the ions, charged and uncharged dendrimer monomer species, and solvent molecules.[50] The second term,

$$\beta\mathscr{F}_{\text{elec}} = \int d\boldsymbol{r}\left[\rho_0\varphi_e(\boldsymbol{r})\Phi(\boldsymbol{r}) - \frac{1}{8\pi l_B}|\nabla\Phi|^2\right], \tag{14}$$

accounts for the electrostatic interactions between the charged entities through the electrostatic potential, $\Phi(r)$ (normalized by k_BT), and the volume fraction of the charged species, $\varphi_e(\boldsymbol{r})$.[40] The third term,

$$\beta\mathscr{F}_{\text{comp}} = \frac{\zeta}{2}\int d\boldsymbol{r}\left[\sum_j \varphi_j(\boldsymbol{r}) - 1\right]^2, \tag{15}$$

enforces a harmonic energy penalty with a strength, ζ, to reduce the magnitudes of the density fluctuations relative to the bulk density, ρ_0 (we assume that only the dendrimer monomers (P), grafted monomers (G), LPE molecules (LPE), and solvent molecules (S) possess volume).[40] The term,

$$\begin{aligned}\beta\mathscr{F}_{\text{conf}} = \ln Q_{\text{PG}} + Q_{\text{LPE}} + \int d\boldsymbol{r} w_P(\boldsymbol{r})\varphi_P(\boldsymbol{r}) + \int d\boldsymbol{r} w_G(\boldsymbol{r})\varphi_G(\boldsymbol{r}) \\ + \int d\boldsymbol{r} w_{\text{LPE}}(\boldsymbol{r})\varphi_{\text{LPE}}(\boldsymbol{r}),\end{aligned} \tag{16}$$

describes the conformational entropy of the grafted dendrimer and linear polyelectrolyte molecules in the external fields $w_P(\boldsymbol{r})$, $w_G(\boldsymbol{r})$, and $w_{\text{LPE}}(\boldsymbol{r})$. In the above, Q_{PG} and Q_{LPE} represent the partition functions of the grafted dendrimer and LPE molecules respectively. To obtain these partition functions, we assume that the conformations of the grafted dendrimers can be described using a continuous Gaussian chain model, while the conformations of the LPE molecules can be described using the Kratky–Porod (KP) model.[40] Below we discuss the models for the continuous Gaussian chains and the semiflexible KP models.

A.2 Continuous Gaussian chain model for conjugated dendrimer

For both models, we use the symbol, "s" to index the segments along the chain contour, $\boldsymbol{r}_{i,j}(s)$, to denote the position in space of the s^{th} segment in the j^{th} ($j = 1\ldots f(f-1)^i$) branch of the i^{th} ($i = 1\ldots g$) generation on the dendrimer molecule and $\boldsymbol{r}_k(s)$ to denote the position of the s^{th} segment on the k^{th} ($k = 1\ldots f(f-1)^g$) grafted chain. The total stretching energy U_0 of the dendrimer and graft molecule in the system is given as:

$$\beta U_0(\boldsymbol{r}) = \frac{3}{2a^2}\sum_{i=0}^{g}\sum_{j=0}^{f(f-1)^i}\int_{s_i}^{s_{i+1}}\left|\dot{\boldsymbol{r}}_{i,j}(s)\right|^2 ds + \frac{3}{2a^2}\sum_{k=0}^{f(f-1)^g}\int_{s_{g+1}}^{s_{\text{end}}}\left|\dot{\boldsymbol{r}}_k(s)\right|^2 ds. \tag{17}$$

The partition function, Q_{PG}, can be determined by calculating the statistical weights of a chain diffusing along its trajectory to a point in space, which are given by $q_{\text{PG}}(\boldsymbol{r}, s)$ and $q^\dagger_{\text{PG}}(\boldsymbol{r}, s)$. The function $q_{\text{PG}}(\boldsymbol{r}, s)$ is calculated by first starting from the $s = 0$ end (center of the dendrimer) and then moving forward in s. In a similar fashion, $q^\dagger_{\text{PG}}(\boldsymbol{r}, s)$ describes the statistical weight of the chain diffusing backward in s, starting from the $s = N_{\text{end}}$ portion of the grafted dendrimer. The partition function of grafted dendrimer chain can then be calculated from:

$$Q_{\text{PG}} = \frac{1}{V}\int d\boldsymbol{r} q^\dagger_{\text{PG}}(\boldsymbol{r}, s = 0), \tag{18}$$

The functions $q_{\text{PG}}(\boldsymbol{r}, s)$ and $q^\dagger_{\text{PG}}(\boldsymbol{r}, s)$ for the dendrimer molecule can be found from the following "diffusion-like" equations:[40]

$$\begin{aligned}\frac{\partial q_{\text{PG}}}{\partial s} = \frac{a^2}{6}\nabla^2 q_{\text{PG}} - [\gamma(s)w_P(\boldsymbol{r}) \\ + (1-\gamma(s))w_G(\boldsymbol{r})]q_{\text{PG}}; q_{\text{PG}}(\boldsymbol{r}, s=0) = \delta(\boldsymbol{r}).\end{aligned} \tag{19}$$

where $\gamma(s) = 1\,\forall\, s \le s_g$, $\gamma(s) = 0\,\forall\, s > s_g$. The "initial" condition in eqn (19) forces the central (0^{th}) monomer to reside at $\boldsymbol{r} = 0$ (the center of the spherical simulation cell). The function $q^\dagger_{\text{PG}}(\boldsymbol{r}, s)$ that runs from the periphery of the dendrimer is given by

$$\begin{aligned}-\frac{\partial q^\dagger_{\text{PG}}}{\partial s} = \frac{a^2}{6}\nabla^2 q^\dagger_{\text{PG}} - [\gamma(s)w_P(\boldsymbol{r}) \\ + (1-\gamma(s))w_G(\boldsymbol{r})]q^\dagger_{\text{PG}}; q^\dagger_{\text{PG}}(\boldsymbol{r}, s=N) = 1.\end{aligned} \tag{20}$$

In order to account for the branching within the dendrimer, we apply the following conditions[60]

$$q^\dagger_{\text{PG}}(\boldsymbol{r}, s_i^-) = [q^\dagger_{\text{PG}}(\boldsymbol{r}, s_i^+)]^{f-1};\ i \le g \tag{21}$$

$$q_{\text{PG}}(\boldsymbol{r}, s_i^+) = q_{\text{PG}}(\boldsymbol{r}, s_i^-)[q^\dagger_{\text{PG}}(\boldsymbol{r}, s_i^+)]^{f-2};\ i \le g \tag{22}$$

where $q^\dagger_{\text{PG}}(\boldsymbol{r}, s_i^-)$ refers to spatially dependent chain propagator for a monomer at a value of s that is infinitesimally smaller than s_i, the value of s at the i^{th} branching point. The above conditions (eqn (21) and (22)) embody the fact that at the dendrimer branch points, the $f-1$ outer generation chains connect. This is analogous to $f-1$ independent particles diffusing to the same point in space at the exact same time.[60] In order to solve for $q_{\text{PG}}(\boldsymbol{r}, s)$ and $q^\dagger_{\text{PG}}(\boldsymbol{r}, s)$, we first determine $q^\dagger_{\text{PG}}(\boldsymbol{r}, s)$ and then subsequently use it *via* eqn (22) to determine $q_{\text{PG}}(\boldsymbol{r}, s)$. For grafted dendrimer molecules, we assume no flux boundary conditions at the center and periphery of the cell ($\nabla q_{\text{PG}}(\boldsymbol{r} = 0, s) = \nabla q_{\text{PG}}(\boldsymbol{r} = \infty, s) = \nabla q^\dagger_{\text{PG}}(\boldsymbol{r} = 0, s) = \nabla q^\dagger_{\text{PG}}(\boldsymbol{r} = \infty, s) = 0$). We employed the Crank–Nicholson finite difference scheme[40,61] to solve the partial differential equations for $q_{\text{PG}}(r, s)$ and $q^\dagger_{\text{PG}}(r, s)$ in eqn (19) and (20) respectively. We solve these equations on a lattice which is non-dimensionalized by $R_g = \sqrt{Na^2/6}$.

A.3 Kratky–Porod model for LPE chains

In the KP model, the bonded interactions are quantified through the elastic bending energy term

$$\beta U_{0,\text{KP}} = \frac{\lambda}{2}\sum_{i=0}^{n_{\text{LPE}}}\int_0^{N_{\text{LPE}}} ds\left|\frac{d\boldsymbol{u}_i(s)}{ds}\right|^2, \tag{23}$$

where $\boldsymbol{u}_i(s) \equiv \boldsymbol{r}_i(s)/ds$ represents the tangent vector to the chain at the contour location s and is constrained to be a unit vector. The term λ represents the bending elasticity of the polymer and is directly proportional to the persistence length of the polymer. In a similar fashion to Q_{PG}, the partition function of the LPE chains, Q_{LPE}, can be calculated from

$$Q_{\text{LPE}} = \int d\boldsymbol{r}\int d\boldsymbol{u}\, q_{\text{LPE}}(\boldsymbol{r}, \boldsymbol{u}, N_{\text{LPE}}), \tag{24}$$

where the field $q_{\mathrm{LPE}}(\boldsymbol{r}, \boldsymbol{u}, s)$ satisfies the equation

$$\frac{\partial q_{\mathrm{LPE}}(\boldsymbol{r}, s)}{\partial s} = -\boldsymbol{u}\cdot\nabla_{\boldsymbol{r}} q_{\mathrm{LPE}} + \frac{1}{2\lambda}\nabla_{\boldsymbol{u}}{}^2 q_{\mathrm{LPE}}(\boldsymbol{r}, s) - w_{\mathrm{LPE}}(r) q_{\mathrm{LPE}}. \qquad (25)$$
$$q_{\mathrm{LPE}}(\boldsymbol{r}, \boldsymbol{u}, s = 0) = 1.$$

The term $q_{\mathrm{LPE}}(\boldsymbol{r}, \boldsymbol{u}, s)$ represents the statistical weight that a wormlike chain experiencing a potential $w_{\mathrm{LPE}}(\boldsymbol{r})$ has its segment s at position $\boldsymbol{r}$ with orientation $\boldsymbol{u}$. For LPE molecules, we assume no flux boundary conditions at the center and periphery of the cell ($\nabla q_{\mathrm{LPE}}(\boldsymbol{r} = 0, \boldsymbol{u}, s) = \nabla q_{\mathrm{LPE}}(\boldsymbol{r} = \infty, \boldsymbol{u}, s) = 0$).

Because the system is spherically symmetric, we can exploit the property that

$$q_{\mathrm{LPE}}(\boldsymbol{r}, \boldsymbol{u}, s) \equiv q_{\mathrm{LPE}}(\boldsymbol{r}, \boldsymbol{u}\cdot\boldsymbol{e}_r, s) \qquad (26)$$

where r denotes the radial distance from the center of the dendrimer and $\boldsymbol{e}_r$ represents the unit radial vector (relative to an origin placed at the center of the dendrimer) at the location $\boldsymbol{r}$. We adopt a local coordinate system centered on $\boldsymbol{r}$, with $\boldsymbol{e}_r$ representing the Z axis and $\boldsymbol{u}\cdot\boldsymbol{e}_r = \cos\theta$, so that eqn (25) can be represented as

$$\frac{\partial q_{\mathrm{LPE}}(\boldsymbol{r}, \theta, s)}{\partial s} = -\cos\theta\frac{\partial q_{\mathrm{LPE}}}{\partial r} + \frac{\sin\theta}{r}\frac{\partial q_{\mathrm{LPE}}}{\partial \theta} + \frac{1}{2\lambda}\frac{1}{\sin\theta}\frac{\partial}{\partial\theta}\left(\sin\theta\frac{\partial q_{\mathrm{LPE}}}{\partial\theta}\right) - w_{\mathrm{LPE}}(r) q_{\mathrm{LPE}}.$$
$$q_{\mathrm{LPE}}(\boldsymbol{r}, \theta, s = 0) = 1. \qquad (27)$$

Eqn (27) forms the starting point for analyzing the configurations of semiflexible polymers in spherically symmetric situations. A convenient way to solve eqn (27) is by expanding $q_{\mathrm{LPE}}(\boldsymbol{r}, \theta, s)$, $q^{\dagger}_{\mathrm{LPE}}(\boldsymbol{r}, \theta, s)$ in terms of Legendre polynomials

$$q_{\mathrm{LPE}}(\boldsymbol{r}, \theta, s) = \sum_l q_{\mathrm{LPE},l}(r, s) P_l(\cos\theta), \qquad (28)$$

where P_l represents the l^{th} order Legendre polynomial. By using the properties of Legendre polynomials, eqn (27) can be transformed into

$$\frac{\partial q_{\mathrm{LPE},l}}{\partial s} = -\frac{l+1}{2l+3}\frac{\partial q_{\mathrm{LPE},l+1}}{\partial r} - \frac{l}{2l-1}\frac{\partial q_{\mathrm{LPE},l-1}}{\partial r} - \frac{(l+1)(l+2)}{2l+3}\frac{q_{\mathrm{LPE},l+1}}{r} + \frac{l(l-1)}{2l-1}\frac{q_{\mathrm{LPE},l-1}}{r} - \frac{l(l+1)}{2\lambda} q_{\mathrm{LPE},l} - w_{\mathrm{LPE}}(r) q_{\mathrm{LPE},l}, \qquad (29)$$

subject to the conditions

$$\nabla q_{\mathrm{LPE},l}(r = 0, s) = 0;\ \ q_{\mathrm{LPE},l}(r, s = 0) = \delta_{l,0}. \qquad (30)$$

To obtain the numerical solution for $q_{\mathrm{LPE},l}(r, s)$, we employ a two-step Lax–Wenderoff (LW) method similar to that suggested by Daoulas and co-workers. Truncation of the Legendre polynomial expansion (eqn (28)) to $l = 6$ was found to ensure sufficient convergence of the density profiles. The presence of large positive w_{LPE} values near the dendrimer core led to oscillations in the density profiles near the dendrimer core, which were more pronounced for increased LPE rigidity. In order to remove oscillations from our system, we used a one step Lax method close to the dendrimer center and transitioned into the two step LW method away from the dendrimer core. The equations were solved by using discretizations in the range of $\mathrm{d}r = 1/30$ and $\mathrm{d}s = 1/2000$.

A.4 Self-consistent equations

The self-consistent equations are found as the saddle point of eqn (12) with respect to the fields $\varphi_{\mathrm{i}}(\boldsymbol{r})$ (where i = P, G, LPE, Na^+, Cl^-, H^+, OH^-, and S), $w_{\mathrm{i}}(\boldsymbol{r})$, and $\Phi(\boldsymbol{r})$. Such a procedure yields:[40]

$$w_{\mathrm{P}}(\boldsymbol{r}) = \zeta(\varphi_{\mathrm{P}}(\boldsymbol{r}) + \varphi_{\mathrm{G}}(\boldsymbol{r}) + \varphi_{\mathrm{LPE}}(\boldsymbol{r}) + \varphi_{\mathrm{S}}(\boldsymbol{r}) - 1) + \alpha_{\mathrm{P}}\ln\left[\frac{1-\alpha(r)}{1-\alpha_{\mathrm{b}}}\right] - \alpha_{\mathrm{P}}, \qquad (31)$$

$$w_{\mathrm{G}}(\boldsymbol{r}) = \zeta(\varphi_{\mathrm{P}}(\boldsymbol{r}) + \varphi_{\mathrm{G}}(\boldsymbol{r}) + \varphi_{\mathrm{LPE}}(\boldsymbol{r}) + \varphi_{\mathrm{S}}(\boldsymbol{r}) - 1), \qquad (32)$$

$$w_{\mathrm{LPE}}(\boldsymbol{r}) = \zeta(\varphi_{\mathrm{P}}(\boldsymbol{r}) + \varphi_{\mathrm{G}}(\boldsymbol{r}) + \varphi_{\mathrm{LPE}}(\boldsymbol{r}) + \varphi_{\mathrm{S}}(\boldsymbol{r}) - 1) + z_{\mathrm{LPE}}\alpha_{\mathrm{LPE}}\Phi(\boldsymbol{r}), \qquad (33)$$

$$w_{\mathrm{S}}(\boldsymbol{r}) = \zeta(\varphi_{\mathrm{P}}(\boldsymbol{r}) + \varphi_{\mathrm{G}}(\boldsymbol{r}) + \varphi_{\mathrm{LPE}}(\boldsymbol{r}) + \varphi_{\mathrm{S}}(\boldsymbol{r}) - 1), \qquad (34)$$

$$-\frac{1}{4\pi l_{\mathrm{B}}\rho_0}\nabla^2\Phi(\boldsymbol{r}) = \sum_{i=\mathrm{ions}} z_i\varphi_i(\boldsymbol{r}) + z_{\mathrm{PH}^+}\alpha_{\mathrm{P}}\alpha(\boldsymbol{r})\varphi_{\mathrm{P}}(\boldsymbol{r}) + z_{\mathrm{LPE}}\alpha_{\mathrm{LPE}}\varphi_{\mathrm{LPE}}(\boldsymbol{r}), \qquad (35)$$

and

$$\alpha(\boldsymbol{r}) = \frac{1}{1 + 10^{\mathrm{p}K_{\mathrm{b,P}} - \mathrm{pOH}}\exp(-z_{\mathrm{OH}^-}\Phi(r))}. \qquad (36)$$

In the above, z_i represents the charge valency of the i^{th} species and

$$\varphi_{\mathrm{P}}(\boldsymbol{r}) = \frac{\eta_{\mathrm{P}}\overline{\varphi}_{\mathrm{P}}}{M(g)Q_{\mathrm{PG}}}\sum_{i=0}^{g}\Omega_i\int_{s_i}^{s_{i+1}}\mathrm{d}s q_{\mathrm{PG}}(\boldsymbol{r}, s) q^{\dagger}_{\mathrm{PG}}(\boldsymbol{r}, s), \qquad (37)$$

$$\varphi_{\mathrm{G}}(\boldsymbol{r}) = \frac{\eta_{\mathrm{G}}\overline{\varphi}_{\mathrm{G}}}{M_{\mathrm{G}}(g)Q_{\mathrm{PG}}}\Omega_g\int_{s_{g+1}}^{s_{\mathrm{end}}}\mathrm{d}s q_{\mathrm{PG}}(\boldsymbol{r}, s) q^{\dagger}_{\mathrm{PG}}(\boldsymbol{r}, s), \qquad (38)$$

$$\varphi_{\mathrm{LPE}}(\boldsymbol{r}) = \eta_{\mathrm{LPE}}\varphi_{\mathrm{LPE,b}}\int_0^{N_{\mathrm{LPE}}}\mathrm{d}s\sum_l\frac{q_{\mathrm{LPE},l}(r, s) q_{\mathrm{LPE},l}(r, N_{\mathrm{LPE}} - s)}{2l+1}, \qquad (39)$$

$$\varphi_{\mathrm{S}}(\boldsymbol{r}) = \varphi_{\mathrm{S,b}}\exp[-w_{\mathrm{S}}(\boldsymbol{r})], \qquad (40)$$

and

$$\varphi_{\mathrm{ion}}(\boldsymbol{r}) = \exp[-\beta\gamma^{\mathrm{o}}_{\mathrm{ion}}]\exp[-z_{\mathrm{ion}}\Phi(\boldsymbol{r})], \qquad (41)$$

where $N = (g+1)n + N_{\mathrm{G}}$ is contour length from the center of the dendrimer to the edge of the grafted chain, $\eta_j = \upsilon_j\rho_0$, with υ_j being the volume of a j^{th} molecule, and Ω_i is the number of branches in the i^{th} generation.

We solve the Poisson–Boltzmann (PB) equation (eqn (35)) in order to obtain $\Phi(\boldsymbol{r})$, and we assume a no flux condition at the center of the cell:

$$\nabla\Phi(\boldsymbol{r}=0)=0. \tag{42}$$

At infinitely large radial values, gradients in $\Phi(\boldsymbol{r})$ are expected to approach zero. However, computational limitations preclude the use of such large cells, and we instead assume that the electrostatic potential decays to zero at the edge of our simulation cell. We a used a cell size of $75R_g$ such that the electrostatic potential could smoothly decay to 0. Random initial values for the fields were applied, and the field values were solved *via* a Picard iteration scheme.[62] We used a convergence criteria which imposed that the largest absolute value of the error in the fields from their self-consistent values was less than or equal to 0.005.

A.5 LPE order parameter

The local orientation of the LPE molecules can be accounted for through the local order parameter, $S(r)$, which is given by

$$S(r)=\left\langle\frac{3\cos^2\theta(r)-1}{2}\right\rangle. \tag{43}$$

where $\theta(r)$ denotes the angles formed between the radial vector emanating from the dendrimer center and the LPE bond vectors at position r. In the SCFT framework, this order parameter is defined as the largest eigen value of the tensorial field

$$\boldsymbol{S}(\boldsymbol{r})=\frac{\int \mathrm{d}s\int \mathrm{d}\boldsymbol{u}\; q_{\mathrm{LPE},l}(r,\boldsymbol{u},s)\frac{1}{2}(3\boldsymbol{uu}-\boldsymbol{I})q_{\mathrm{LPE},l}(r,\boldsymbol{u},N_{\mathrm{LPE}}-s)}{\int \mathrm{d}s\int \mathrm{d}\boldsymbol{u}\; q_{\mathrm{LPE},l}(r,\boldsymbol{u},s)q_{\mathrm{LPE},l}(r,\boldsymbol{u},N_{\mathrm{LPE}}-s)}. \tag{44}$$

By applying eqn (26) and performing a Legendre polynomial expansion of q_{LPE} and $q^{\dagger}_{\mathrm{LPE}}$, one may obtain a scalar value of S as a function of r. We note that $S(r)$ is able to vary from $S(r)=1$, where the LPE chain is completely oriented along the $\boldsymbol{e}_r$ vector to $S(r)=-1/2$, where the LPE chain is completely oriented tangentially along the $\boldsymbol{e}_\theta$.

Acknowledgements

This work was supported in part by a grant from Robert A. Welch Foundation (Grant F1599) and National Science Foundation (DMR 1005739). The authors acknowledge the Texas Advanced Computing Center (TACC) at The University of Texas at Austin for providing computing resources that have contributed to the research results reported within this paper.

References

1 J. F. KukowskaLatallo, A. U. Bielinska, J. Johnson, R. Spindler, D. A. Tomalia and J. R. Baker, *Proc. Natl. Acad. Sci. U. S. A.*, 1996, **93**, 4897–4902.
2 H. Yoo, P. Sazani and R. L. Juliano, *Pharm. Res.*, 1999, **16**, 1799–1804.
3 D. Luo, K. Haverstick, N. Belcheva, E. Han and W. M. Saltzman, *Macromolecules*, 2002, **35**, 3456–3462.
4 J. S. Choi, K. Nam, J. Park, J. B. Kim, J. K. Lee and J. Park, *J. Controlled Release*, 2004, **99**, 445–456.
5 M. L. Patil, M. Zhang, S. Betigeri, O. Taratula, H. He and T. Minko, *Bioconjugate Chem.*, 2008, **19**, 1396–1403.
6 G. S. Yu, Y. M. Bae, H. Choi, B. Kong, I. S. Choi and J. S. Choi, *Bioconjugate Chem.*, 2011, **22**, 1046–1055.
7 Y. J. Tsai, C. C. Hu, C. C. Chu and I. Toyoko, *Biomacromolecules*, 2011, **12**, 4283–4290.
8 A. M. Chen, L. M. Santhakumaran, S. K. Nair, P. S. Amenta, T. Thomas, H. X. He and T. J. Thomas, *Nanotechnology*, 2006, **17**, 5449–5460.
9 K. Fant, E. K. Eshjorner, A. Jenkins, M. C. Grossel, P. Lincoln and B. Norden, *Mol. Pharm.*, 2010, **7**, 1734–1746.
10 K. Fant, B. Norden and P. Lincoln, *Biochemistry*, 2011, **50**, 1125–1127.
11 F. Tack, A. Bakker, S. Maes, N. Dekeyser, M. Bruining, C. Elissen-Roman, M. Janicot, M. Brewster, H. M. Janssen, B. F. M. De Waal, P. M. Fransen, X. Lou and E. W. Meijer, *J. Drug Targeting*, 2006, **14**, 69–86.
12 Y. Tang, Y.-B. Li, B. Wang, R.-Y. Lin, M. van Dongen, D. M. Zurcher, X.-Y. Gu, M. M. Banaszak Holl, G. Liu and R. Qi, *Mol. Pharm.*, 2012, **9**, 1812–1821.
13 O. Taratula, O. B. Garbuzenko, P. Kirkpatrick, I. Pandya, R. Savla, V. P. Pozharov, H. X. He and T. Minko, *J. Controlled Release*, 2009, **140**, 284–293.
14 D. A. Tomalia, A. M. Naylor and W. A. Goddard, *Angew. Chem., Int. Ed. Engl.*, 1990, **29**, 138–175.
15 Y. Y. Cheng, Z. H. Xu, M. L. Ma and T. W. Xu, *J. Pharm. Sci.*, 2008, **97**, 123–143.
16 D. Astruc, E. Boisselier and C. Ornelas, *Chem. Rev.*, 2010, **110**, 1857–1959.
17 W.-d. Tian and Y.-q. Ma, *Chem. Soc. Rev.*, 2013, **42**, 705–727.
18 P. K. Maiti and B. Bagchi, *Nano Lett.*, 2006, **6**, 2478–2485.
19 V. Vasumathi and P. K. Maiti, *Macromolecules*, 2010, **43**, 8264–8274.
20 D. Ouyang, H. Zhang, H. S. Parekh and S. C. Smith, *Biophys. Chem.*, 2011, **158**, 126–133.
21 L. B. Jensen, G. M. Pavan, M. R. Kasimova, S. Rutherford, A. Danani, H. M. Nielsen and C. Foged, *Int. J. Pharm.*, 2011, **416**, 410–418.
22 B. Nandy and P. K. Maiti, *J. Phys. Chem. B*, 2011, **115**, 217–230.
23 K. Karatasos, P. Posocco, E. Laurini and S. Pricl, *Macromol. Biosci.*, 2012, **12**, 225–240.
24 P. Welch and M. Muthukumar, *Macromolecules*, 2000, **33**, 6159–6167.
25 S. V. Lyulin, A. A. Darinskii and A. V. Lyulin, *Macromolecules*, 2005, **38**, 3990–3998.
26 S. V. Lyulin, A. A. Darinskii and A. V. Lyulin, *Phys. Rev. E: Stat., Nonlinear, Soft Matter Phys.*, 2008, **78**, 041801.
27 S. V. Larin, S. V. Lyulin, A. V. Lyulin and A. A. Darinskii, *Polym. Sci., Ser. A*, 2009, **51**, 459–468.
28 S. V. Larin, A. A. Darinskii, A. V. Lyulin and S. V. Lyulin, *J. Phys. Chem. B*, 2010, **114**, 2910–2919.

29 W. D. Tian and Y. Q. Ma, *Macromolecules*, 2010, **43**, 1575–1582.
30 J. S. Klos and J. U. Sommer, *J. Chem. Phys.*, 2011, **134**, 204902.
31 J. S. Klos and J. U. Sommer, *Macromol. Theory Simul.*, 2012, **21**, 448–460.
32 S. P. Hong, A. U. Bielinska, A. Mecke, B. Keszler, J. L. Beals, X. Y. Shi, L. Balogh, B. G. Orr, J. R. Baker and M. M. B. Holl, *Bioconjugate Chem.*, 2004, **15**, 774–782.
33 A. Mecke, I. J. Majoros, A. K. Patri, J. R. Baker, M. M. B. Holl and B. G. Orr, *Langmuir*, 2005, **21**, 10348–10354.
34 K. Jain, P. Kesharwani, U. Gupta and N. K. Jain, *Int. J. Pharm.*, 2010, **394**, 122–142.
35 T. Zhou and S. B. Chen, *Macromolecules*, 2005, **38**, 8554–8561.
36 T. Zhou and S. B. Chen, *Macromolecules*, 2006, **39**, 6686–6692.
37 H. Lee and R. G. Larson, *Macromolecules*, 2011, **44**, 2291–2298.
38 N. D. Sonawane, F. C. Szoka and A. S. Verkman, *J. Biol. Chem.*, 2003, **278**, 44826–44831.
39 T. Lewis, V. Pryamitsyn and V. Ganesan, *J. Chem. Phys.*, 2011, **135**, 204902.
40 G. Fredrickson, *The Equilibrium Theory of Inhomogeneous Polymers*, Oxford University Press, 2005.
41 R. C. Hedden and B. J. Bauer, *Macromolecules*, 2003, **36**, 1829–1835.
42 P. Carbone, F. Negri and F. Muller-Plathe, *Macromolecules*, 2007, **40**, 7044–7055.
43 P. Carbone and F. Muller-Plathe, *Soft Matter*, 2009, **5**, 2638–2647.
44 S. Huissmann, A. Wynveen, C. N. Likos and R. Blaak, *J. Phys.: Condens. Matter*, 2010, **22**, 232101.
45 G. M. Pavan, M. A. Mintzer, E. E. Simanek, O. M. Merkel, T. Kissel and A. Danani, *Biomacromolecules*, 2010, **11**, 721–730.
46 V. Ganesan, L. Khounlavong and V. Pryamitsyn, *Phys. Rev. E: Stat., Nonlinear, Soft Matter Phys.*, 2008, **78**, 051804.
47 D. T. Wu, G. H. Fredrickson, J. P. Carton, A. Ajdari and L. Leibler, *J. Polym. Sci., Part B: Polym. Phys.*, 1995, **33**, 2373–2389.
48 I. Borukhov and L. Leibler, *Macromolecules*, 2002, **35**, 5171–5182.
49 U. Nagpal, F. A. Detcheverry, P. F. Nealey and J. J. de Pablo, *Macromolecules*, 2011, **44**, 5490–5497.
50 R. Nap, P. Gong and I. Szleifer, *J. Polym. Sci., Part B: Polym. Phys.*, 2006, **44**, 2638–2662.
51 P. Gong, J. Genzer and I. Szleifer, *Phys. Rev. Lett.*, 2007, **98**, 018302.
52 M. J. Uline, Y. Rabin and I. Szleifer, *Langmuir*, 2011, **27**, 4679–4689.
53 K. N. Witte, S. Kim and Y. Y. Won, *J. Phys. Chem. B*, 2009, **113**, 11076–11084.
54 J. Hur, K. N. Witte, W. Sun and Y. Y. Won, *Langmuir*, 2010, **26**, 2021–2034.
55 K. B. David and P. Landau, *A guide to Monte Carlo simulations in statistical physics*, Cambridge University Press, 2009.
56 N. Metropolis, A. W. Rosenbluth, M. N. Rosenbluth, A. H. Teller and E. Teller, *J. Chem. Phys.*, 1953, **21**, 1087–1092.
57 T. Lewis and V. Ganesan, *J. Phys. Chem. B*, 2012, **116**, 8269–8281.
58 T. Lewis and V. Ganesan, *Soft Matter*, 2012, **8**, 11817–11830.
59 J. K. Wolterink, J. van Male, M. Daoud and O. V. Borisov, *Macromolecules*, 2003, **36**, 6624–6631.
60 G. M. Grason and R. D. Kamien, *Phys. Rev. E: Stat., Nonlinear, Soft Matter Phys.*, 2005, **71**, 051801.
61 W. H. Press, S. A. Teukolsky, W. T. Vetterling and B. P. Flannery, *Numerical Recipies: The Art of Scientific Computing*, Cambridge University Press, 2007.
62 G. H. Fredrickson, V. Ganesan and F. Drolet, *Macromolecules*, 2002, **35**, 16–39.